Physica Scripta

PAPER

Structural, optical, and morphological evaluation of PVA/Bi-Ni oxide-rGO nanocomposite casted films for optical devices applications

RECEIVED
4 March 2024

REVISED
14 June 2024

ACCEPTED FOR PUBLICATION
16 July 2024

PUBLISHED
25 July 2024

T S Soliman[1,2], **Ahmed I Abdel-Salam**[3], **Mohamed Morsy**[3,4], **Hanan A Matar**[3,5] and **A Khalid**[6]

[1] Institute of Natural Sciences and Mathematics, Ural Federal University, Ekaterinburg 620000, Russia
[2] Physics Department, Faculty of Science, Benha University, Benha 13518, Egypt
[3] Nanotechnology Research Centre (NTRC), The British University in Egypt (BUE), Suez Desert Road, El Sherouk City, Cairo 11837, Egypt
[4] Building Physics and Environment Institute, Housing & Building National Research Center (HBRC), Dokki, Giza 12311, Egypt
[5] Physics Department, Faculty of Science, Helwan University, 11792 Helwan, Cairo, Egypt
[6] Department of Basic Engineering Sciences, Faculty of Engineering at Shoubra, Benha University, Cairo, Egypt

E-mail: tarek.attia@fsc.bu.edu.e.g

Keywords: PVA, Bi_2O_3-NiO-rGO, UV-visible spectroscopy, optical bandgap, refractive index

Abstract

Herein, the polyvinyl alcohol (PVA) films doped with various concentrations of Bi_2O_3-NiO-rGO (BNG) nanoparticles were prepared through casting method. BNG nanoparticles were synthesized first using the co-precipitation method and then loaded into the polymer matrix. Various techniques like X-ray diffraction, Raman spectroscopy, and optical microscopes were used to determine the PVA's structure after BNG nanoparticle additives. The thermal stability of the PVA's film after the additive BNG nanoparticles was examined using the DSC technique. Furthermore, the optical parameters including bandgap energy (E_g), Urbach energy (E_U), refractive index (n), optical conductivity, and optical dielectric constants were investigated via the absorbance and transmission data recorded using UV-visible spectroscopy. In addition, the photoemission spectra of the PVA matrix were determined after the inclusion of BNG nanoparticles. The E_g value decreases from 5.57 eV to 3.94 eV and from 4.8 eV to about 1.98 eV for direct and indirect transitions, respectively. While the E_U value increases from 0.39 eV for pure PVA to about 3.23 eV for PVA: 4%BNG. The refractive index grows with the insertion of BNG to the PVA from 1.387 for pure PVA to about 5.157 for PVA: 4% BNG, which is a good suggestion for optical glasses applications. In addition, the increase in optical dielectric constants and optical conductivity with rising the BNG nanoparticle concentrations in the PVA matrix was confirmed. Such enhancement suggests the use of prepared samples in optical device applications.

1. Introduction

In recent years, polymer-incorporating nanofillers have been a subject of growing research interest due to their unique optical, electrical, and mechanical capabilities [1]. Several avenues are being pursued to continue improving the characteristics of polymer materials. It is accomplished by several methods such as doping with various nanoparticles, changing the concentrations until they reach optimum one, and changing the shape of the filler or its size [2, 3]. The purpose of enhancing the characteristics of polymer nanocomposites is to raise their refractive index, density, and reduce the bandgap, as the polymeric nanocomposites with high refractive index and outstanding optical clarity are now attracting a lot of scientific attention due to their prospective uses in lenses, optical filters, and light-emitting diodes [4].

Recently, polyvinyl alcohol (PVA) has been used as a host matrix for many nanoparticles. PVA is a polar material that contains a C-C chain [5, 6], responsible for the semi-crystallinity nature of the PVA structure, attached with OH groups that can interact with cations of the fillers through it and form nanocomposite

polymer [7]. Although PVA has good optical qualities, its refractive index is low (~1.409 at $\lambda = 500$nm) [8]. Previously, several metal oxides, including $BaTiO_3$ [9], SiO_2, La_2ZnO [10], graphene-reduced graphene oxides [11], Fe_2O_3 [12], NiO [13], and $KMnO_4$ [14] were utilized in PVA-matrices to improve their optical parameters and raising the composite density and refractive index for optical applications [2].

Bi_2O_3 is a p-type heavy metal-oxide-semiconductor with a lower bandgap (2.8 eV) that can be easily activated by visible light, besides its promising photocatalyst characteristic and high refractive index [15–17]. This make Bi_2O_3 to be used in creative applications like solar cells, gas sensor, catalyst, radiation shielding, and full cells [18]. Bi_2O_3 was used as a nanofiller to improve the properties of the polymer matrix [16, 17, 19, 20]. Muthamma *et al* [16] studied the impact of bismuth (Bi) ions on the optical properties of PVA films and revealed that Bi ions additives in the PVA matrix enhance their optical and shielding properties. Abunahel *et al* [17] observed that an additive of Bi_2O_3 nanoparticles to the epoxy-PVA composite film improves their shielding properties, and the x-ray attenuation by the composite was increased with increasing the loading content of the Bi_2O_3. Early research on the effects of Bi_2O_3 with carbon quantum dots on the morphological and optical characteristics of PVA films revealed that raising the concentration of Bi_2O_3 in the matrix improved the optical parameters [19]. Also, Bi_2O_3 was found to enhance the optical properties of PVA/PPy (polypyrrole) blend film [21].

Recently, PVA system doped with graphene or its derivatives (graphene oxide (GO) and reduced GO (rGO)) have been studied and concluded that the GO/rGO improves the absorbance of the PVA film and reduces its optical bandgap energy [22–24]. Loading the polymer composite system with a small amount of graphene material enhances the matrix properties [25], besides improving the photochemical stability of the matrix that is combined with it [26–29]. Besides, the Ni ions are characterized by their unique optical properties, as the metal oxides doped with Ni ions causes an enhancement in their photocatalytic activity and the photo response of the material by preventing charge carriers from recombining on the photocatalyst's surface [30, 31]. Recently, Ni was reinforced in the PVA matrix and a great influence on their optical parameters was observed, and their ability to be used in nonlinear optical applications [32]. Also, Ni was added to the polyvinylpyrrolidone (PVP) matrix and improved their thermal stability and electrical conductivity by loading low concentration [2]. Bi_2O_3/CuO/GO nanocomposite material for biomedical and optical applications was recently synthesized by combining Bi_2O_3 with CuO and GO in a composite material, as the GO influences the optical bandgap energy of Bi_2O_3 [33]. So, using a composite material combining Ni ions and rGO sheets on the Bi_2O_3 to synthesize a new composite material to be used as a filler in the PVA matrix to enhance their optical properties is expected to show new and fascinating properties.

Herein, the novelty is the use of Bi_2O_3-NiO-rGO nanoparticles in the PVA matrix for the first time. Doping Bi_2O_3 with Ni was found to improve the photocatalysts properties and reduces the bandgap [31]. Moreover, the presence of reduced graphene oxide (rGO) in the matrix will enhance the optical features of the polymer films, as reported earlier [27, 34] . Our expectation is that the optical properties will be improved and be better than that in case of Bi_2O_3 alone without doping. This paper focuses on creating novel polymer films doped with various Bi_2O_3-NiO-rGO contents. The fabricated PVA/Bi_2O_3-NiO-rGO films are characterized by XRD, Raman spectroscopy, and polarized optical microscope. In addition, the optical properties via UV-visible spectrophotometer are investigated.

2. Experimental

2.1. Materials

Bismuth (III) nitrate pentahydrate (molecular weight (M_w) 485.07 g mole^{-1}), nickel nitrate hexahydrate ($M_w = 290.79$ g mole^{-1}), polyethylene glycol (PEG 8000), graphene oxide (GO), sodium hydroxide ($M_w =$ 40 g mole^{-1}) used in this study were analytical grade, without any further purification. Polyvinyl alcohol (PVA), boasting a $M_w = 1 \times 10^6$, was acquired from the Qualikem Company.

2.2. Bi_2O_3-NiO-rGO nanoparticles preparation

The Bi_2O_3-NiO-rGO (BNG) nanoparticles were synthesized using the co-precipitation method. Typically, bismuth (III) nitrate pentahydrate (0.1 M) and graphene oxide (GO) with ratio 5:1 were dissolved in 100 ml de-ionized water, then 0.25 gm of polyethylene glycol was added till obtaining a homogeneous mixture by heating at 80 °C. Then, nickel nitrate hexahydrate (0.1 M) was added to the mix. After that, a sodium hydroxide solution (2 M) was added dropwise until it reached a pH value of about 10, then left the reaction for one hour at 80 °C. The precipitated powder was washed with deionized water several times and dried at 80 °C/12 h. Finally, the obtained powder was calcined at 400 °C/2 h.

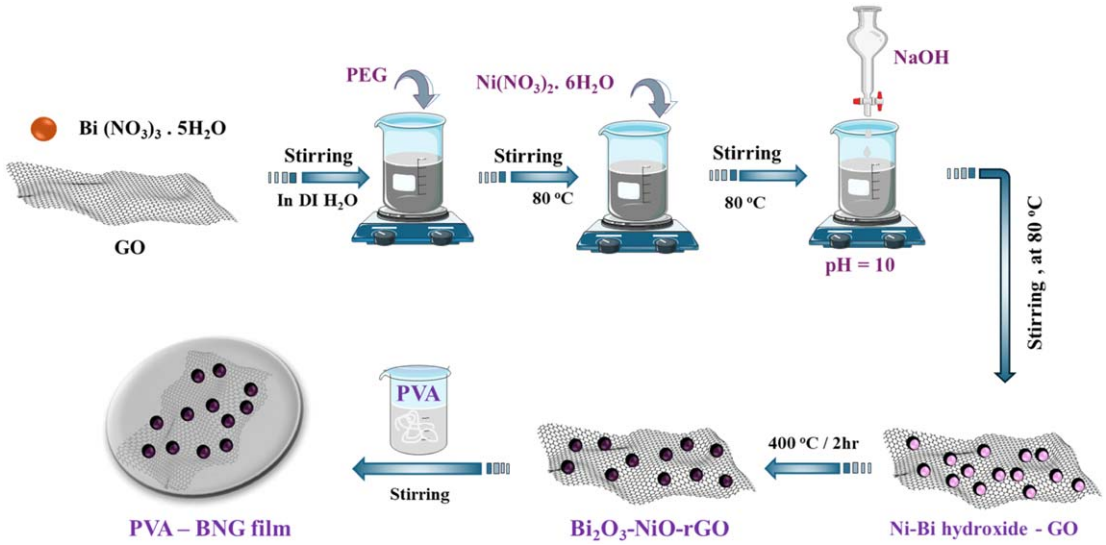

Scheme 1. Schematic diagram for the experimental work.

2.3. PVA: BNG films preparation and characterizations

Various concentrations of the prepared BNG NPs (0, 1, 2, 3, and 4 wt%) were added to the PVA solutions, which were prepared by dissolving PVA powder in distilled water at 70 °C through mixing under a magnetic stirrer for about 4 h. The mix solutions (PVA: BNG) were sonicated by high intense ultrasonication probe for about 3 min. Then, the solutions were poured into petri dishes and left for a week (at 25 °C) for drying. The obtained films were removed from the dishes and utilized for the appropriate analysis. The PVA: BNG films have equal thickness of about ~100 μm. The prepared films were applied to measurements using X-ray diffraction (XRD, Bruker-D8), polarized optical microscope (OLYMPUS-BX51), Raman spectroscopy (WiTec-Alpha-300-AR), and UV-visible spectroscopy (Cary-5000). The DSC thermograms were conducted using DSC131 Evo instruments under nitrogen environment protection. Photoluminescence (PL) measurements were conducted at room temperature with laser wavelength 375 nm via Lumina Fluorescence Spectrometer- Thermo-Scientific. Field-emission scanning electron microscopy (FE-SEM) and energy-dispersive X-ray (EDX) were used to study the morphology and the elemental composition on the surface of the PVA: BNG films structure using a Quattro S FE-SEM (Thermo Scientific, Waltham, MA, USA) at 10 kV.

3. Results and discussion

3.1. XRD analysis

XRD spectrum of the prepared BNG nanoparticles is illustrated in figure 1(a). The diffraction peaks noticed at 26.25°, 32.68°, 45.68°, 46.86°, and 54.52° are linked to (201), (002), (222), (400), and (203) diffraction plans, that are attributed to alpha-Bi_2O_3 (JCPDS# 71-0465) [35–37]. In addition, there is no peak was observed for Ni due to their lower content in the composite and this matched well with the literature [35]. In line with the literature [38–40], the rGO shows a weak broad peak around 12.4° and 24.3°, which could be due to the overlapping with Bi_2O_3 and NiO.

XRD spectra for pristine and reinforced PVA samples are illustrated in figure 1(b). It shows the known characteristic hump of the PVA at about 2θ~ 20°, which is indexed to the (101) diffraction plane [41, 42]. This broad hump reflects the semi-crystalline phase of the PVA, which is caused due to the presence of the C-C chains in the PVA matrix [5, 6].

The BNG NPs additives to PVA reduce the hump (2θ~20°) intensity with broadening. It reflects the destruction of the main structure of the polymer with new bond creation between the inserted BNG nanoparticles and the molecules of PVA. Furthermore, the diffraction peaks of the inserted NPs are observed at 26.37°, 32.76°, 46.99°, and 54.62° related to the BNG NPs, which agreed well with the literature [31, 36]. In addition, the peak observed at 12.44° and 24.68° is related to the rGO inside the BNG nanocomposite, which matched well with the literature [43, 44]. These peaks grow and slightly shift with increasing BNG concentration in the matrix, which is associated with the agglomerations of the BNG NPs and the growth of the particle size. The full-width at half-maximum (FWHM), diffraction peaks positions (2θ), and *d*-spacing for PVA: BNG films are listed in table 1.

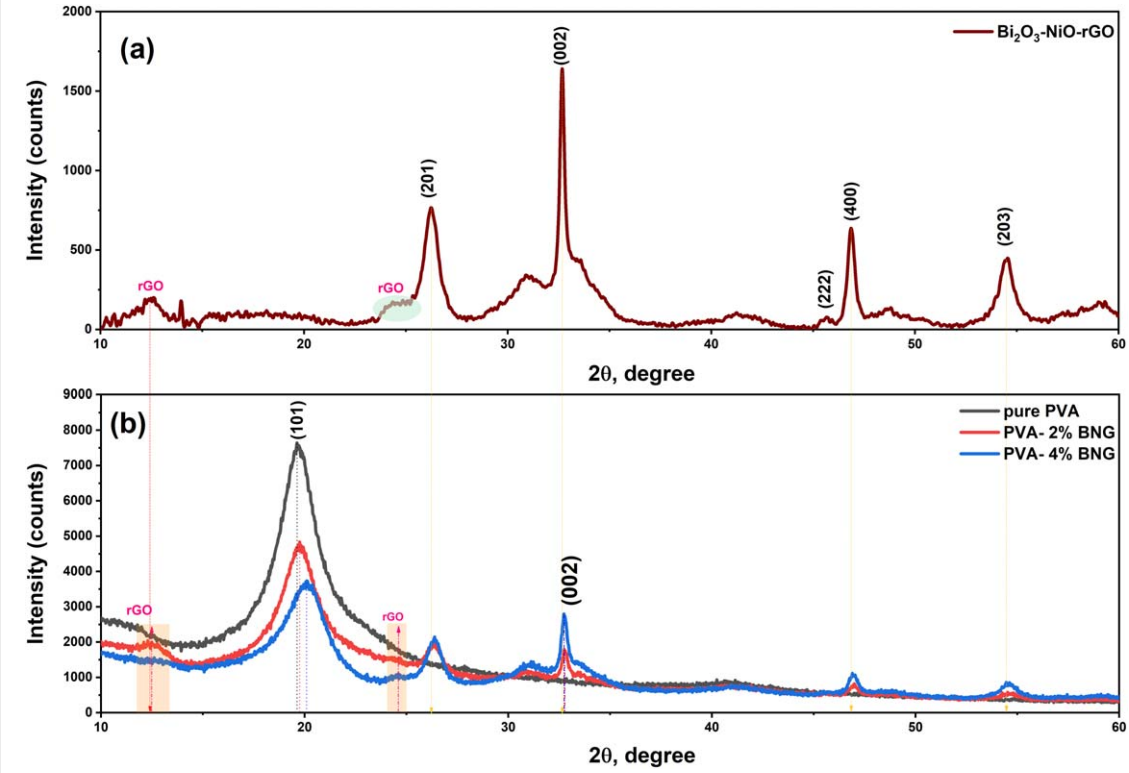

Figure 1. XRD patterns of (a) BNG nanoparticles and (b) PVA: BNG films.

Table 1. XRD structural parameters for PVA: BNG films.

Sample ID	diffraction plane	FWHM (°)	2θ (°)	D (nm)	ε	δ (nm^{-2})	d-spacing (Å)
Pure PVA	(101)	2.7499	19.62	3.06	0.069	0.1067	4.5198
PVA-2%BNG	(101)	2.7557	19.75	3.06	0.069	0.1071	4.4916
	(002)	0.9417	32.76	9.18	0.014	0.0119	2.7318
PVA-4%BNG	(101)	2.8576	20.14	2.95	0.070	0.1149	4.4055
	(002)	0.6068	32.74	14.23	0.009	0.0049	2.7334

As the BNG concentration in the PVA matrix increases, the PVA distinct peak (101) position moves towards the higher angle, the FWHM for the (101) plane increases from 2.7499 (pure PVA) to 2.7557 (PVA:2%BNG), and 2.8576 (PVA:4%BNG). In addition, the d-spacing of the (101) plane decreases, indicating the shrinking of the interplanar distance of the polymer chains. This observation indicates the decrease in PVA semi-crystallinity caused by the destruction of the H-bonds in the PVA matrix and the formation of H-bonds between BNG nanoparticles and OH-groups of PVA. The FWHM for the (002) plane decreased from 0.9417 to about 0.6068 for PVA: 2%BNG and PVA: 4% BNG, respectively, and the d-spacing for the (002) plane slightly increased, as seen in table 1. This confirms the growth of BNG nanoparticle size, which is ascribed to the nanoparticle accumulations with increasing its content into the PVA. The structural parameters like the average particle size (D), dislocation density (δ), and micro-strain (ε) are affected after the inclusion of the BNG nanoparticles in the PVA matrix, which are evaluated as follows [45],

$$D = \frac{0.9\lambda}{\beta \cos\theta} \tag{1}$$

$$\varepsilon = \frac{\beta}{4\tan\theta} \tag{2}$$

$$\delta = \frac{1}{D^2} \tag{3}$$

From table 1, the $D_{(101)}$ value and d-spacing decrease, while the ε and δ values increase with the increase in BNG concentrations. This could be related to the decrement in the interatomic distance between the molecules

with the inclusion of BNG nanoparticles in the polymer matrix.The pure BNG nanoparticles have a $D_{(002)}$ value of 25 nm. Moreover, the $D_{(002)}$ value (in the PVA matrix) and d-spacing increase as the BNG concentration increases. This can be ascribed to the aggregations as the reason for such a change in the matrix.

3.2. Morphology analysis

Under the bright filed optical microscope, optical microscope (OM) and polarized optical microscope (POM), the PVA: BNG films were analyzed to clarify the distributions of the BNG nanoparticles in the PVA matrix, as shown in figure 2. The clear and smoothed image shown in figure 2(a) is for the pure PVA, without any cracks or voids. Figures 2(b)–(e) shows the PVA films reinforced with various BNG concentrations. At lower concentrations, the BNG nanoparticles are distributed uniformly inside the PVA matrix. The BNG nanoparticles accumulate at higher concentrations and form big particles.

Under the polarized light, a dark background is seen for the pure PVA (figure 2(a)'), and spherulite bright particles distributed uniformly start to be clear with reinforcing with lower concentration 1%BNG (figure 2(b)'). It represents the Bi_2O_3 and Ni nanoparticles as the rGO sheets are dark in the background, as reported in the literature [46].

The number of bright particles increases with increasing the BNG contents (2, 3, and 4%BNG). These particles tend to be attracted to each other and aggregate to form grains. The distance between these bright particles decreases and becomes denser and more crowded due to increasing BNG content in the PVA matrix, as shown in figures 2(c')-(e'). The electrostatic forces between the nanoparticles and each other are the reason for the formation of the aggregations, besides the long time (around a week) that it takes to form the PVA films [17].

Figure 3 displays the SEM image, particle size distribution (Histogram), and EDX analysis of the PVA: BNG films.

The SEM image of PVA- 2% BNG film, figure 3(a), shows a dark background related to the polymer and white particles with some agglomerations related to the doped material. The distribution of these particles, as shown in figure 3(b), is in the nanoscale with a minimum of 28 nm and big particles up to approximately 370 nm. With the increase of the BNG in the PVA matrix up to 4%, figure 3(c), the agglomeration increases, and the doped material is flower-shaped particles were produced, that were uniformly dispersed densely into the PVA matrix. Such behavior is in line with the literature [15, 35]. As shown in the particle distribution, figure 3(d), tiny particles in the range of 42 nm and big particles flower-shaped in the range of 2.5 μm. These big particles are formed because of agglomerations. This agglomeration was caused due to the electrostatic force between the nanoparticles and each other's, which took place during evaporation of the solvent, it matched well with literature [17]. A further EDX analysis was performed on the PVA-4% BNG film to confirm the presence of the BNG nanoparticles in the PVA matrix (figure 3(e)). It shows the signals of nickel (Ni), bismuth (Bi), oxygen (O), and carbon (C) elements, where the C element refers to the PVA matrix and the rGO.

3.3. Raman analysis

Structural analysis of the polymer films was further verified by Raman spectroscopy. Figure 4 shows the Raman scattering of the pure PVA and PVA: BNG films.

The Raman spectrum reveals that the PVA thin film has characteristic peaks at 856, 920, and 1440 cm^{-1} [47]. After the inclusion of about 2% and 4% of BNG nanoparticles into the PVA, the Raman spectra revealed additional characteristic peaks at 102, 145, and 155 cm^{-1} that are characteristic for the Bi_2O_3 [48], while the peaks at 200 and 315 cm^{-1} are characteristic for the NiO [49, 50]. These results are in good accordance with the Raman modes characterized for Bi_2O_3 and NiO in previous studies [48–50]. It was noted that there are no distinct peaks related to the graphene oxide, which could be due to its small quantity in the prepared nanoparticles.

3.4. DSC analysis

The differential scanning calorimetry (DSC) measurements have been carried out for pure PVA, PVA: 2% BNG, and PVA: 4% BNG samples from room temperature up to 250 °C, as shown in figure 5.

The DSC thermogram for the pure PVA showed two endothermic peaks, one at 106.4 °C associated with the glass transition temperature (T_g), and the other at 197.5 °C associated with the melting temperature (T_m). After doping the PVA matrix with the BNG nanoparticles, these degrees were shifted to higher temperatures, as shown in figure 5. These shifts in the T_g and T_m to a higher temperature of the PVA: BNG films indicate that the BNG caused an enhancement in the PVA film's thermal stability. This is likely due to the formation of robust intermolecular interactions between the BNG NPs and the PVA molecule. This outcome matched both the Raman and XRD spectra.

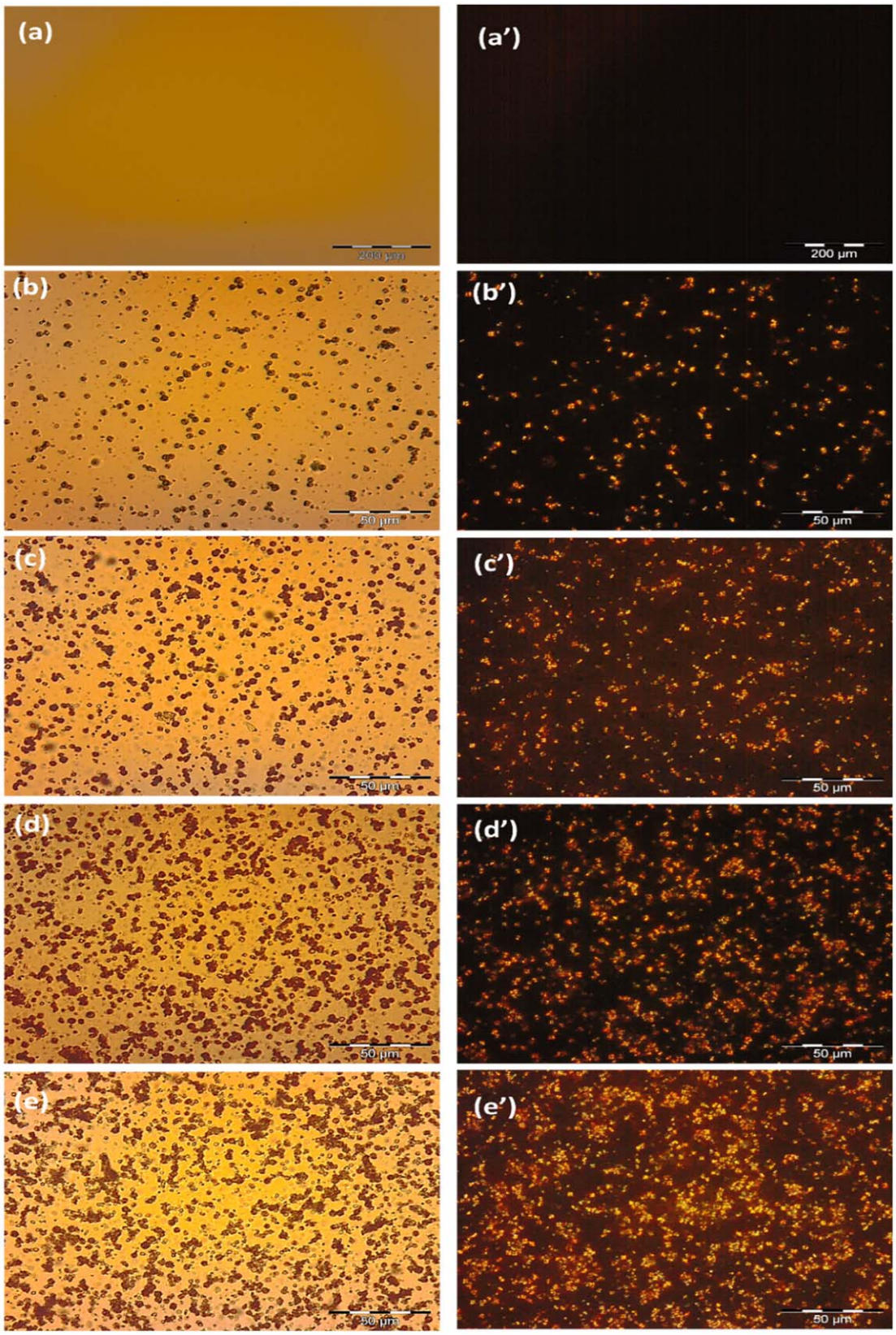

Figure 2. OM (a, b, c, d, e) and POM (a', b', c', d', e') images for all samples; (a, a') pure PVA, (b, b') 1%, (c, c') 2%, (d, d') 3%, and (e, e') 4% BNG NPs. Magnification 40x.

3.5. Optical properties

3.5.1. UV-visible spectra, optical bandgaps, and Urbach energy.

Recognizing a substance's optical properties relies mainly on its electronic energy band structure. The optical absorbance spectrum supplies fundamental data about the optical bandgap of the material. Figure 6 illustrates

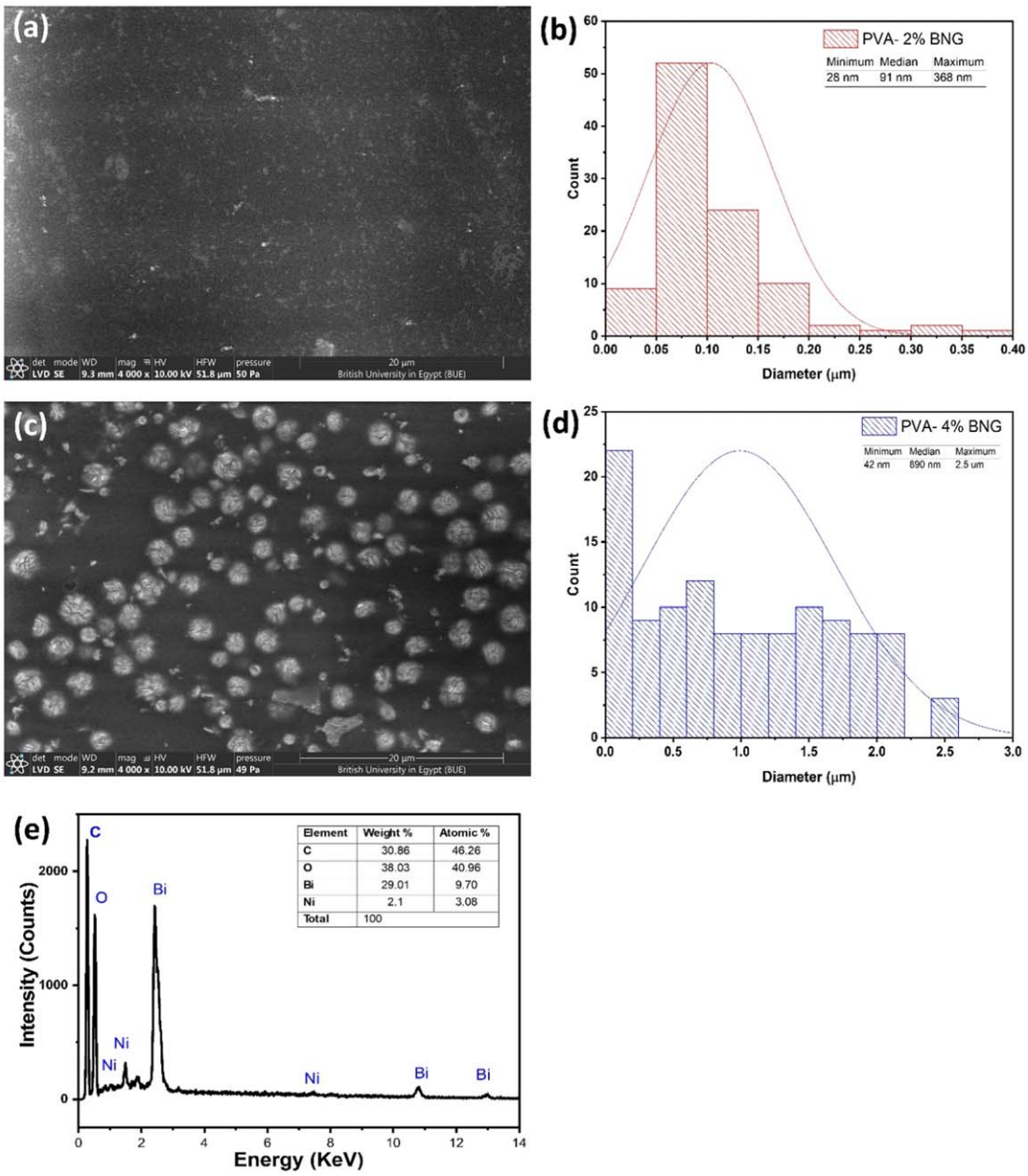

Figure 3. SEM and histogram of; (a, b) PVA: 2% BNG, (c, d) PVA: 4% BNG film, and (e) EDX of PVA: 4% BNG film.

the UV-visible spectra (measured experimentally, transmittance (**T**) and absorbance (**A**)) for PVA: BNG films.

A pure PVA film is highly transparent and doesn't show absorption peaks in the visible region. While the transmittance for the doped films shows a broad hump in the visible zone, which is caused due to the presence of the BNG NPs, as shown in figure 6(a). Furthermore, the transparency of the polymer film decreases gradually from 91% for pure PVA to about 57% (PVA-1% BNG), 30% (PVA-2% BNG), 21% (PVA-3% BNG), and 12% (PVA-4% BNG), as the BNG concentration increases in the polymer matrix.

An absorption peak can be observed in the ultraviolet region, making it a suitable material for use as a polarizer, as shown in figure 6(b) [21, 51]. For pure PVA film, absorption peaks at the backbone were scanned at 279nm (π-π^*transition) and 332nm (n-π^*transition) [21, 52]. A sharp absorption edge in the 205–250 nm range was observed, which matched the PVA bandgap and indicated the semi-crystallinity of PVA [53]. This outcome was confirmed by XRD analysis. Figure 6(b) depicts a redshift in the absorption edge with an increase in the BNG concentration. This could be due to the formation of inter-/intra-molecular hydrogen bonding between BNG NPs and OH groups of the PVA [53]. The absorbance of all polymer films declines as the wavelength increases; it additionally rises as the BNG NPs content rises. Moreover, the polymer film absorbance increases as the wavelength increases from 650 nm towards the near-infrared region, which is caused by the presence of Ni in the

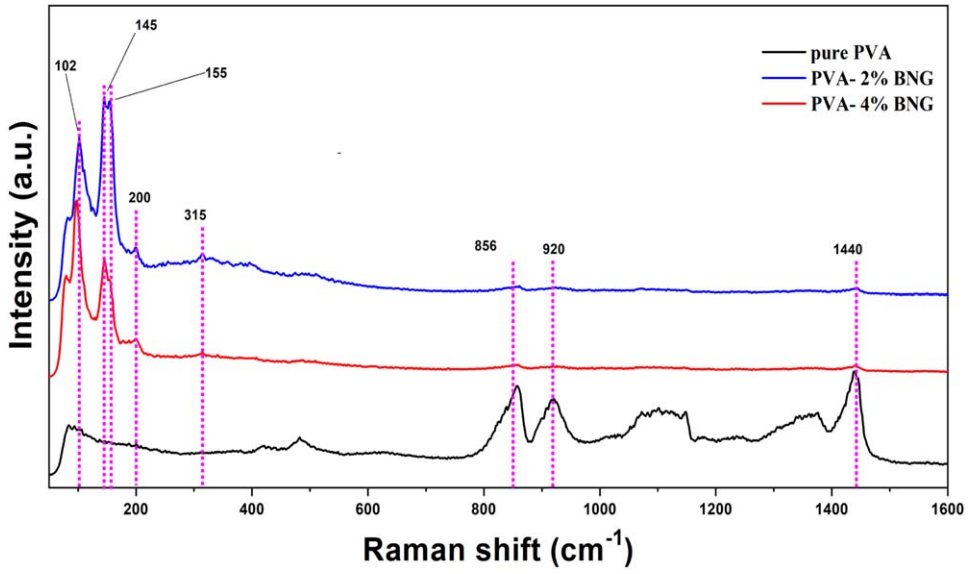

Figure 4. Raman spectra for pure PVA, PVA-2%BNG, and PVA-4%BNG films.

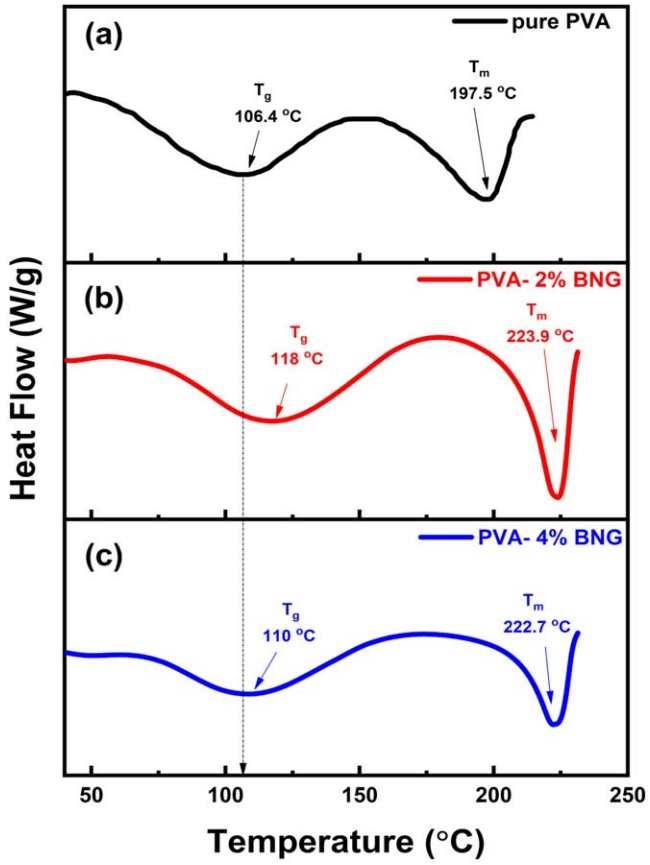

Figure 5. DSC curves of (a) pure PVA, (b) PVA: 2% BNG, and PVA: 4% BNG films.

BNG nanoparticles, which coincides with the literature [54]. The absorbance increases due to BNG NPs additives and the growth in their sizes, which is caused by its accumulation inside the polymer matrix, as well as the existence of rGO sheets that absorb more energy [45, 55]. The prepared nanocomposite films exhibit promising properties as a UV absorber.

The reduction in bandgap energy of materials is unmistakably revealed by the redshift observed in the edge of the absorption spectra. By utilizing Tauc's relation, we can accurately determine the type of electron transition

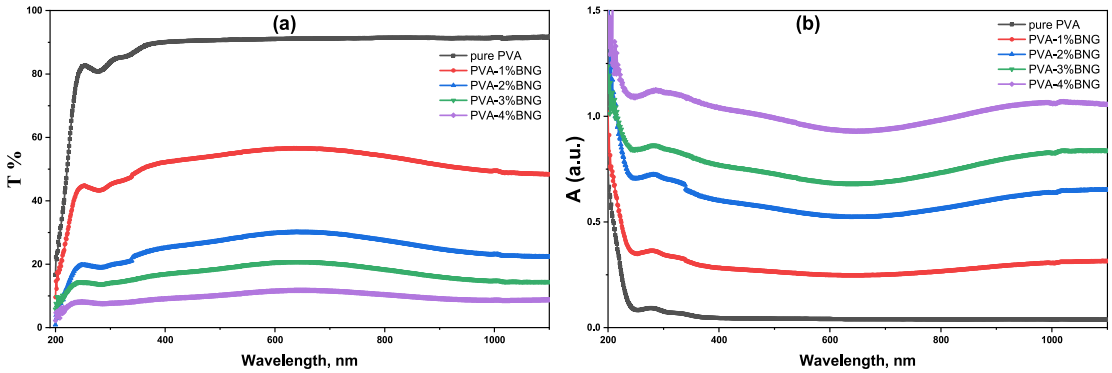

Figure 6. UV-visible spectra (a)Transmittance and (b)Absorbance spectra for all samples.

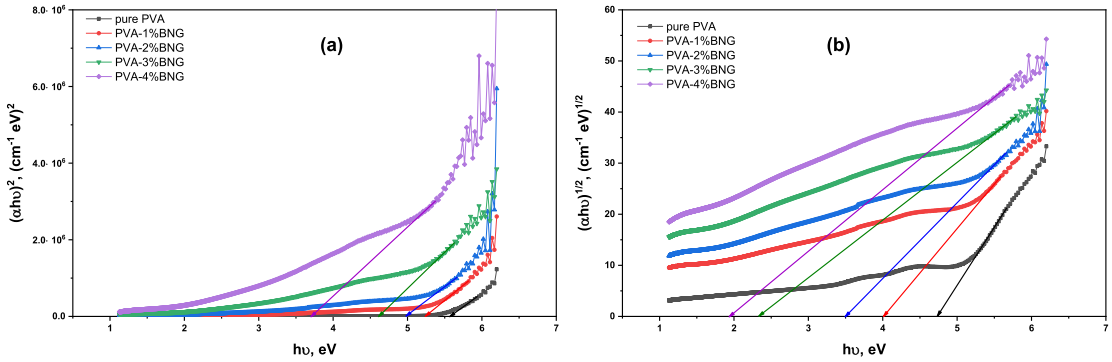

Figure 7. Plot of $(\alpha h\upsilon)^2$ (a) and $(\alpha h\upsilon)^2$ (b) versus $h\upsilon$ for all samples.

Table 2. Optical parameter for PVA: BNG films.

Sample ID	E_{gd} (eV)	E_{gi} (eV)	E_U (eV)	n ($\lambda = 600$nm)
pure PVA	5.57	4.73	0.39	1.387
PVA-1% BNG	5.23	4.00	0.94	2.263
PVA-2% BNG	4.96	3.50	1.59	3.337
PVA-3% BNG	4.61	2.33	2.56	4.006
PVA-4% BNG	3.70	1.94	3.23	5.172

and evaluate the bandgap energy as follows [56, 57];

$$(\alpha h\nu)^2 = B_1(h\nu - E_{gd}) \tag{4}$$

$$(\alpha h\nu)^{1/2} = B_2(h\nu - E_{gi}) \tag{5}$$

where α, h, υ, B_1, B_2, E_{gd}, and E_{gi} represent the coefficient of absorption, Planck's-constant, light-frequency, B_1&B_2 are constants depending on the transition probability, and the bandgap energy for direct (E_{gd}) and indirect (E_{gi}) transitions, respectively. The E_{gd} and E_{gi} values are estimated by extending the straight line of the relation between $(\alpha h\upsilon)^2$ and $(\alpha h\upsilon)^{1/2}$ as a function of photon energy ($h\upsilon$), as shown in figure 7.

Table 2 summarizes the extracted E_{gd} and E_{gi} values. It shows that, for both cases, direct and indirect, as the concentration of the BNG increases, the bandgap decreases as well. The E_{gd} decreases from 5.57eV to about 3.70eV and E_{gi} from 4.73eV to about 1.97eV for pure PVA and PVA-4% BNG films, respectively. This is caused by the amorphous structure of PVA, which is linked to the multiple localized states formed in the bandgap among the valence and conduction bands as the outcome of PVA impurities [55]. The fresh states support capture and emit electrons between the bands [58]. By contrasting the acquired data with the PVA film-doped Bi_2O_3 [19], it is possible to determine that doping with a lower BNG nanoparticle content—up to 4 wt%—decreases the bandgap energy to 3.70 eV, which is better than the bandgap of 5.13 eV obtained by the

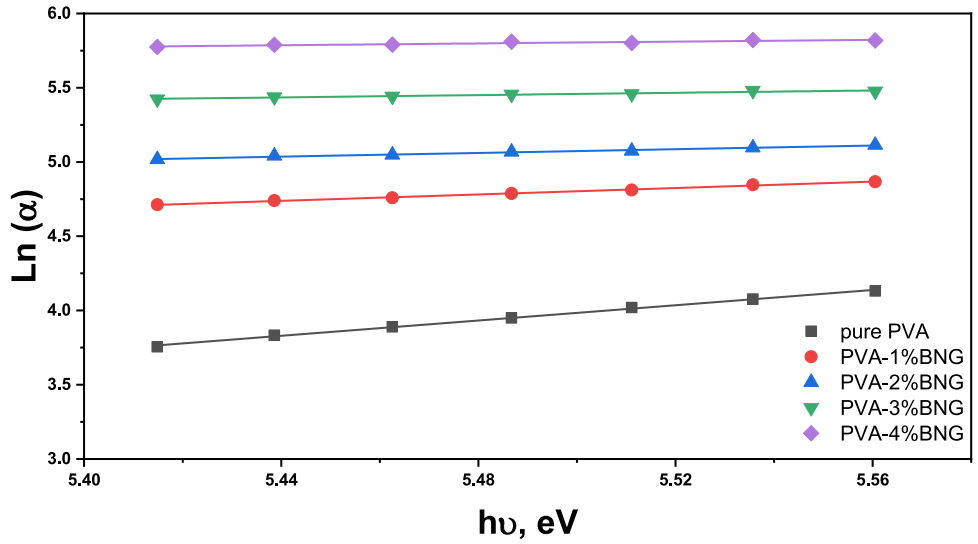

Figure 8. Plot of Ln(a) versus hu for all samples.

Bi_2O_3-doped PVA—up to 3 wt%. This result illustrates how the addition of rGO and Ni ions to a composite containing Bi2O3 increases absorbance and lowers the matrix's bandgap energy.

All the films exhibited an extended tail at the end of the absorption edge in their spectra. This is ascribed to the impurities present in the material, which lead to the creation of new states and a reduction in the distance between the valance and conduction bands. The band tail width, i.e., Urbach energy (E_U), can be calculated by applying the following formula [58]:

$$\alpha = \alpha_o \exp(h\upsilon/E_U) \tag{6}$$

where αo is constant. Figure 8 illustrates the straight-line section of the Ln(α) as a function in (hυ) for PVA: BNG films.

The reciprocal of the slope was used to estimate the E_U values for both the pure PVA and the doped films (see table 2). The E_U value gradually increases from 0.39 eV (pure PVA) to 3.23 eV (PVA:4%BNG). An increase in E_U values indicates a rise in film disorder and the formation of new levels within the forbidden zone [57]. Such an increase in E_U value is a testament to the bandgap reduction of the papered films and makes it a potential material for organic-electronic applications.

3.5.2. Refractive index and extinction coefficient

The successful use of optical materials hinges on two critical variables: the extinction coefficient (k) and refractive index (n). Understanding and optimizing these variables are essential for achieving desired results in optical applications. The (n) and (k) of the films are obtained via the following formulas [58],

$$n = \left(\frac{1+R}{1-R}\right) + \sqrt{\frac{4R}{(1-R)^2} - k^2} \tag{7}$$

$$k = \frac{\alpha\lambda}{4\pi} \tag{8}$$

The development of integrated optical devices is highly dependent on the refractive index (n), which arises mainly from the electronic polarization of ions. Figure 9(a) illustrates how the value of 'n' varies with incident-light wavelength (λ). The BNG additives to the PVA matrix increased the nanocomposite's density, as proved in OM images, leading to slower light penetration [58, 59]. By including more BNG, the n value of PVA increases significantly (see inset of figure 9(a)). This means that PVA with higher BNG content can potentially have better optical properties, making it a more effective and efficient solution for various applications in coating for displays and glasses [60, 61].

The extinction coefficient is the key to unlocking the energy potential of substance molecules as they absorb and scatter light. Figure 9(b) depicts the k values versus the wavelength for different BNG content. The k value of PVA: BNG films is directly proportional to the absorption coefficient, which increases with higher concentrations of BNG. Hence, an increase in BNG concentration leads to an increase in the k value of PVA: BNG films. This makes it a highly efficient and effective material for various applications. The extinction

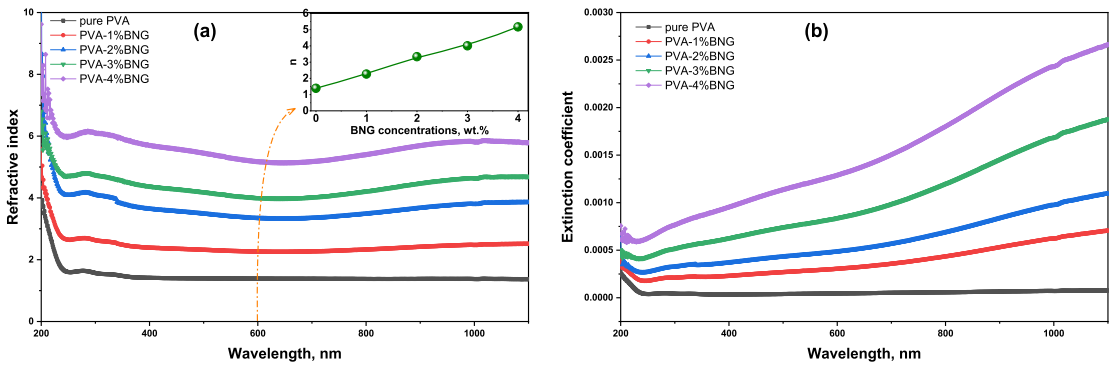

Figure 9. Plots of (a) n and (b) k as versus (λ) for all samples.

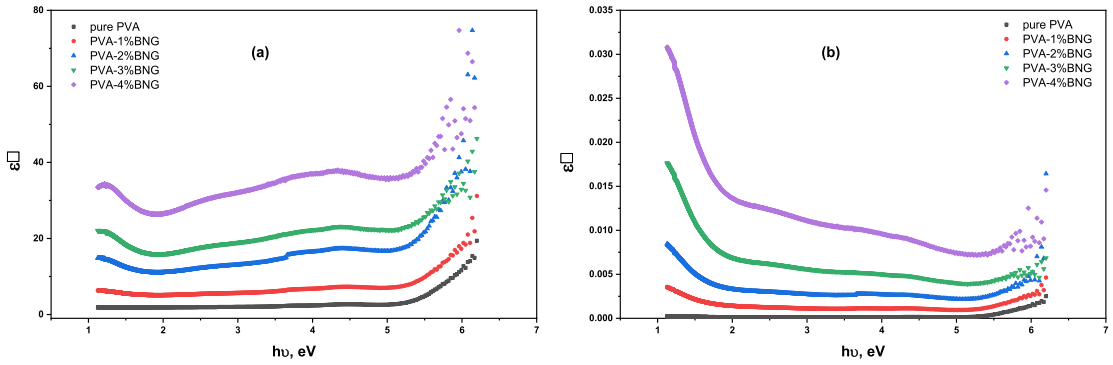

Figure 10. Plots of (a) ε' and (b) ε'' versus hυ for all samples.

coefficient declines with increasing the wavelength, indicating that the incident photon energy is sufficient to stimulate an electron [58, 59].

3.5.3. Optical dielectric parameters and optical conductivity.

The complex dielectric-constant (ε) is a fundamental property of the material, and it has two components: real (ε') and imaginary (ε''), as indicated in the equation below [13],

$$\varepsilon = \varepsilon' + i\varepsilon'' \tag{9}$$

The real part (ε') represents light dispersion within the substance and the imaginary part (ε'') illustrates the absorbed energy generated by dipole moment movement, and it can be computed through the n and k values as follows [52],

$$\varepsilon' = n^2 - k^2 \tag{10}$$

$$\varepsilon'' = 2nk \tag{11}$$

Figure 10 depicts the dependence of (ε') and (ε'') on photon energy (hυ) for PVA: BNG films. The ε' and ε'' values increase as the BNG concentration increases. This trend is an outcome of a modification in the PVA band structure. As the amount of BNG grows, various states are created in the forbidden gap. An increase in (ε') and (ε'') values is associated with defects and structural disorder at greater photon energies owing to polarization [58].

The optical conductivity (σ_{opt}) of a material reflects the effect of the induced current density on the electric field created at random frequencies [58]. The movement of free charge carriers as an effect of the electromagnetic photon beam generates electron excitation, triggering optical conductivity. And this parameter can be computed through the following relation [57, 58],

$$\sigma_{opt} = \frac{n\alpha c}{4\pi} \tag{12}$$

where c denotes light speed. Figure 11 illustrates the fluctuation of σ_{opt} with (hυ) for the PVA: BNG films.

The σ_{opt} value increases as the BNG concentration increases. The σ_{opt} value is of order 10^{10} S^{-1} for pure PVA, and it was increased of order of about 10^{12} S^{-1} for PVA doped with 4% BNG NPs. This could be explained

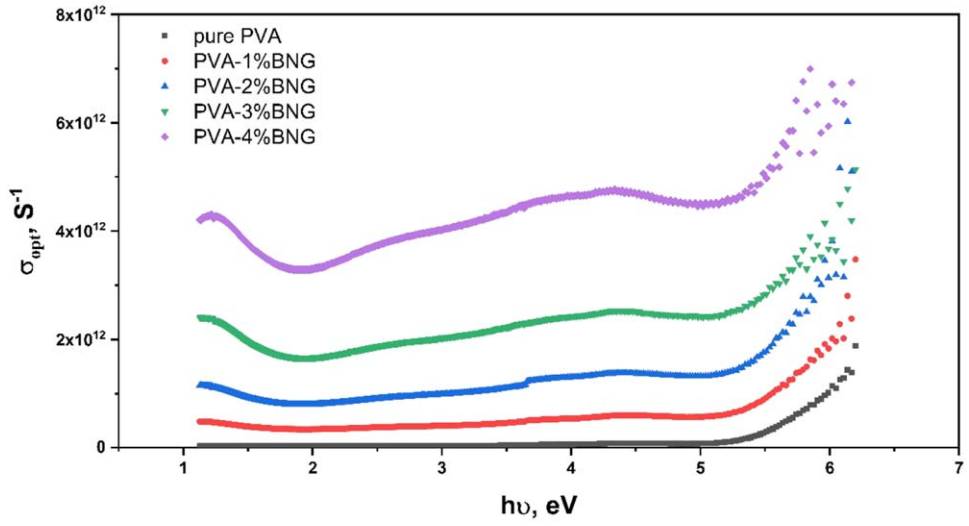

Figure 11. The σ_{opt} versus (hυ) for all samples.

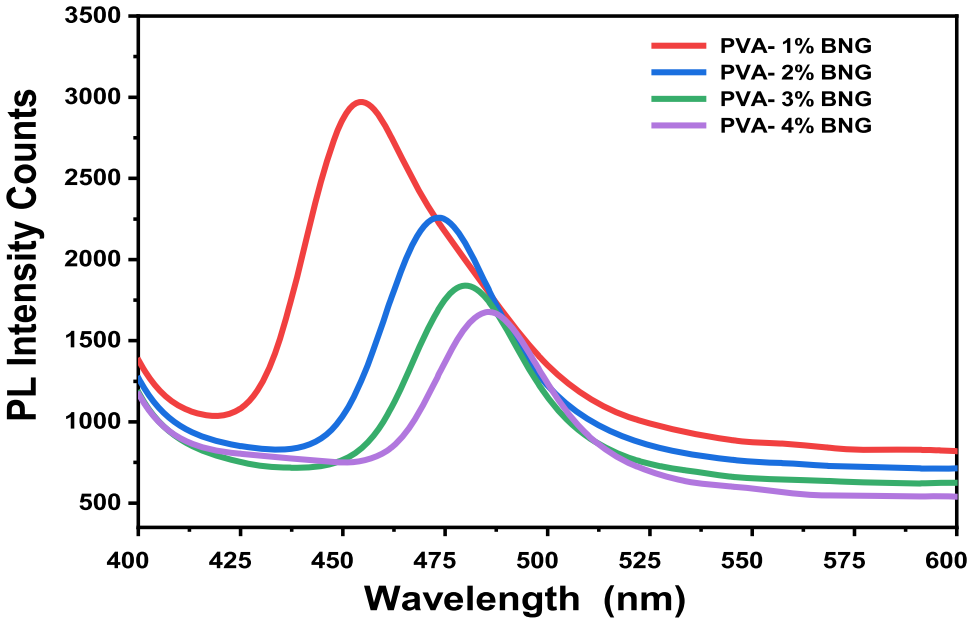

Figure 12. Photoluminescence emission spectra for all samples.

by an increase in the number of free charge carriers in various regions that absorb photon energy and release more free electrons [57].

3.6. Photoluminescence (PL) analysis

Figure 12 depicts the PL emission spectra of PVA-BNG nanocomposite films at excitation wavelength $\lambda_{exc.} = 375$ nm. The PVA does not have an emission peak, based on data from previous work [9]. After doping with 1 wt% BNG nanoparticle, a photoemission peak was observed at 454 nm. This peak decreases in intensity with redshift towards a higher wavelength as the BNG nanoparticle content increases in the PVA matrix. The reduction in peak intensity with the increase in BNG nanoparticles can be attributed to the reduction in hole–electron recombination rate, as they are directly proportional to each other's [62]. The photoemission peak redshifted to 473, 780, and 485 nm for the PVA doped with 2, 3, and 4 wt% BNG, respectively. The redshift of emissions spectra may be due to BNG NPs additives and the growth in their sizes, which is caused by their accumulation inside the polymer matrix [63]. The photocatalytic activity of the materials is enhanced by the low recombination rate and reduced energy gap.

4. Conclusion

The Bi_2O_3-NiO-rGO nanoparticles were prepared through the co-precipitation method, and PVA-Bi_2O_3-NiO-rGO films were obtained via the casting technique. The PVA semi-crystallinity and its modification after the insertion of Bi_2O_3-NiO-rGO nanoparticles was confirmed by XRD. The Raman analysis confirmed the presence of the NiO and Bi_2O_3 characteristics modes after complexation with the PVA. The Bi_2O_3-NiO-rGO nanoparticles were efficiently disseminated in the PVA films with little aggregations. The DSC curves demonstrate that adding Bi_2O_3-NiO-rGO nanoparticles to the matrix enhanced the PVA film's thermal stability. The optical bandgap reduction and increase of the Urbach energy with increasing the Bi_2O_3-NiO-rGO nanoparticles in the PVA attest to the creation of localized states in the polymer film's forbidden zone. Moreover, the interatomic distances decrease because of the rise in the film density, causing an increase in the refractive index and suggesting that the present films are viable candidates for optical applications. The optical dielectric parameters and conductivity increase as the Bi_2O_3-NiO-rGO nanoparticle concentration increases in the PVA. Reducing emission intensities in the PL spectrum verified that the spectral studies matched the decreased rate of electron–hole recombination. Moreover, the photocatalytic activity of the materials is enhanced by the low recombination rate and reduced energy gap Generally, the PVA/Bi_2O_3-NiO-rGO films are promising for various organic optoelectronic applications.

Data availability statement

All data that support the findings of this study are included within the article (and any supplementary files).

ORCID iDs

T S Soliman https://orcid.org/0000-0001-7372-4761

References

[1] Verma R K, Kesarwani S, Xu J and Davim J P 2023 *Polymer Nanocomposites: Fabrication to Applications* (Taylor & F, CRC Press) (https://doi.org/10.1201/9781003343912)
[2] Pascariu P, Airinei A, Grigoras M, Vacareanu L and Iacomi F 2015 Metal-polymer nanocomposites based on Ni nanoparticles and polythiophene obtained by electrochemical method *Appl. Surf. Sci.* **352** 95–102
[3] Stepanov A L 2018 *Optical Properties of Polymer Nanocomposites With Functionalized Nanoparticles* (Elsevier Inc.)
[4] Al-Gunaid M Q A, Saeed A M N, H.M G and Basavarajaiah S 2020 Impact of nano-perovskite La2CuO4 on dc-conduction, opto-electrical sensing and thermal behavior of PVA nanocomposite films *Polym. Technol. Mater.* **59** 469–83
[5] Ali H E, Morad I, Algarni H, El-Desoky M M, Khairy Y, Zahran H Y and Yahia I S 2021 Structure analysis and nonlinear/linear optical properties of PVAOH/Si composites for low-cost optical technologies and limiting absorption *J. Mater. Sci., Mater. Electron.* **32** 4466–79
[6] Zhu Y S, Wang X J, Hou Y Y, Gao X W, Liu L L, Wu Y P and Shimizu M 2013 A new single-ion polymer electrolyte based on polyvinyl alcohol for lithium ion batteries *Electrochim. Acta* **87** 113–8
[7] Abdullah O G, Aziz S B, Omer K M and Salih Y M 2015 Reducing the optical band gap of polyvinyl alcohol (PVA) based nanocomposite *J. Mater. Sci., Mater. Electron.* **26** 5303–9
[8] Soliman T S and Abouhaswa A S 2020 Synthesis and structural of Cd0.5Zn0.5F2O4 nanoparticles and its influence on the structure and optical properties of polyvinyl alcohol films *J. Mater. Sci., Mater. Electron.* **31** 9666–74
[9] Soliman T S, Zaki M F, Hessien M M and Elkalashy S I 2021 The structure and optical properties of PVA-BaTiO3 nanocomposite films *Opt. Mater. (Amst).* **111** 110648
[10] Soliman T S, Hessien M M and Elkalashy S I 2022 Structural, thermal, and optical properties of polyvinyl alcohol films doped with La2ZnOx nanoparticles *J. Non. Cryst. Solids.* **580** 121405
[11] Yilmaz Dogan H, Altin Y and Bedeloğlu A Ç 2022 Fabrication and properties of graphene oxide and reduced graphene oxide reinforced Poly(Vinyl alcohol) nanocomposite films for packaging applications *Polym. Polym. Compos.* **30** 1–11
[12] Parthasarathy V, Selvi J, Senthil Kumar P, Anbarasan R and Mahalakshmi S 2021 Evaluation of mechanical, optical and thermal properties of PVA nanocomposites embedded with Fe2O3 nanofillers and the investigation of their thermal decomposition characteristics under non-isothermal heating condition *Polym. Bull.* **78** 2191–210
[13] Shaalan N M, Hanafy T A and Rashad M 2021 Dual optical properties of NiO-doped PVA nanocomposite films *Opt. Mater. (Amst).* **119** 111325
[14] Abdullah O G, Aziz S B and Rasheed M A 2016 Structural and optical characterization of PVA:KMnO4 based solid polymer electrolyte *Results Phys.* **6** 1103–8
[15] Sharma A, Sharma S, Kumar N, Diery W A, Moujaes E A, Tahir M and Singh P 2023 Co+2, Ni+2 and Cu+2 incorporated Bi2O3 nano photocatalysts: synthesis, DFT analysis of band gap modification, adsorption and photodegradation analysis of rhodamine B and Triclopyr *Environ. Res.* **233** 116478
[16] Muthamma M V, Bubbly S G and Narendranath K C S 2019 Poly (vinyl alcohol)–bismuth oxide composites for X-ray and γ -ray shielding applications *J. Appl. Polym. Sci.* **136** 47949
[17] Abunahel B M, Shahrim I, Nurul M and Noor Z 2018 Characteristics of X-ray attenuation in nano-sized bismuth oxide / epoxy-polyvinyl alcohol (PVA) matrix composites *Appl. Phys. A* **124** 1–7

[18] Jarka P, Tański T, Matysiak W, Krzemiński Ł, Hajduk B and Bilewicz M 2017 Manufacturing and investigation of surface morphology and optical properties of composite thin films reinforced by TiO 2 , Bi 2 O 3 and SiO 2 nanoparticles *Appl. Surf. Sci.* **424** 206–12
[19] Kavgacı M and Eskalen H 2023 Morphology , structure and optical properties of PVA nanocomposites reinforced with bismuth oxide nanoparticles and carbon quantum dots *J. Mater. Sci., Mater. Electron.* **34** 1229
[20] Li Z, Zhang H and Bergman B 2008 Synthesis and characterization of nanostructured Bi 2 O 3 -doped cerium oxides fabricated by PVA polymerization process *Ceram. Int.* **34** 1949–53
[21] Irfan M, Aslam M and Ali Z 2023 Gamma irradiation protection via flexible polypyrrole coated bismuth oxide nanocomposites *Polym. Bull.* **80** 791–807
[22] Goumri M, Venturini J W, Bakour A, Khenfouch M and Baitoul M 2016 Tuning the luminescence and optical properties of graphene oxide and reduced graphene oxide functionnalized with PVA *Appl. Phys. A* **3** 1–8
[23] Badawi A, Mersal G A M, Shaltout A A, Boman J, Alsawat M and Amin M A 2021 Exploring the structural and optical properties of FeS filled graphene/PVA blend for environmental-friendly applications *J. Polym. Res.* **28** 270
[24] Kuilla T, Bhadra S, Yao D, Kim N H, Bose S and Lee J H 2010 Recent advances in graphene based polymer composites *Prog. Polym. Sci.* **35** 1350–75
[25] Alsulami Q A and Rajeh A 2023 Modification and development in the microstructure of PVA/CMC-GO/Fe3O4 nanocomposites films as an application in energy storage devices and magnetic electronics industry *Ceram. Int.* **49** 14399–407
[26] Chakraborty M, Kadir E S and Gayen R N 2023 Enhanced UV photo-detection properties of graphene oxide incorporated transparent TiO2 thin films in Schottky configuration *Ceram. Int.* **49** 20651–61
[27] Martin M, Prasad N, Sivalingam M M, Sastikumar D and Karthikeyan B 2018 Optical, phonon properties of ZnO–PVA, ZnO–GO–PVA nanocomposite free standing polymer films for UV sensing *J. Mater. Sci., Mater. Electron.* **29** 365–73
[28] de Lima A H *et al* 2020 Origin of optical bandgap fluctuations in graphene oxide *Eur. Phys. J. B* **93** 105
[29] Ebrahimi Naghani M, Neghabi M, Zadsar M and Abbastabar Ahangar H 2023 Synthesis and characterization of linear/nonlinear optical properties of graphene oxide and reduced graphene oxide-based zinc oxide nanocomposite *Sci Rep.* **13** 1–10
[30] Skutina L S, Vylkov A A, Kuznetsov D K, Medvedev D A and Shur V Y 2019 Tailoring Ni and Sr2Mg0.25Ni0.75MoO6−δ Cermet Compositions for Designing the Fuel Electrodes of Solid Oxide Electrochemical Cells *Energies.* **12** 2394
[31] Singh S and Sharma R 2018 Bi2O3/Ni-Bi2O3 system obtained via Ni-doping for enhanced PEC and photocatalytic activity supported by DFT and experimental study *Sol. Energy Mater. Sol. Cells* **186** 208–16
[32] Soliman T S, Vshivkov S A and Elkalashy S I 2020 Structural, linear and nonlinear optical properties of Ni nanoparticles—Polyvinyl alcohol nanocomposite films for optoelectronic applications *Opt. Mater. (Amst).* **107** 110037
[33] Qayyum A, Batool Z, Fatima M, Buzdar S A, Ullah H, Nazir A, Jabeen Q, Siddique S and Imran R 2022 Antibacterial and *in vivo* toxicological studies of Bi2O3/CuO/GO nanocomposite synthesized via cost effective methods *Sci Rep.* **12** 14287
[34] Badawi A and Alharthi S S 2022 The optical, electrical and mechanical performance of metal oxides incorporated PVA/rGO blend: effect of metal oxide type *Appl. Phys. A Mater. Sci. Process.* **128** 1–15
[35] Meng Q and Yin Z 2019 Visible light responsive Ni-doped micro/nanostructured Bi2O3 microspheres for photocatalytic denitrification of fuel oil *Mendeleev Commun.* **29** 672–4
[36] Durmu Ş, Uslu İ and Tunç T 2011 Synthesis and characterization of boron-doped Bi 2 O 3 - La 2 O 3 fiber derived nanocomposite precursor *J. Polym. Res.* **18** 1999–2004
[37] Correia F and Ribeiro J M 2020 Photocatalytic Bi2O3/TiO2:N thin films with enhanced surface area and visible light activity *Coatings.* **10** 445
[38] Morsy M, Abdel-Salam A I, Mostafa M and Elzwawy A 2022 Promoting the humidity sensing capabilities of titania nanorods/rGO nanocomposite via de-bundling and maximizing porosity and surface area through lyophilization *Micro Nano Eng.* **17** 100163
[39] Abdel-Aal S K, Ionov A, Mozhchil R N and Naqvi A H 2018 Simple synthesis of graphene nanocomposites MgO–rGO and Fe2O3–rGO for multifunctional applications *Appl. Phys. A Mater. Sci. Process.* **124** 1–10
[40] Abid, Sehrawat P, Islam S S, Mishra P and Ahmad S 2018 Reduced graphene oxide (rGO) based wideband optical sensor and the role of Temperature, Defect States and Quantum Efficiency *Sci Rep.* **8** 3537
[41] Badawi A, Mersal G , A M, Shaltout A , A, Boman J, Alsawat M and Amin M A 2021 Exploring the structural and optical properties of FeS filled graphene/ PVA blend for environmental-friendly applications *J. Polym. Res.* **28** 270
[42] Karthikeyan B, Hariharan S, Sasidharan A, Gayathri V, Arun T, Akbari-Fakhrabadi A and Madhumitha C 2019 Optical, vibrational and fluorescence recombination pathway properties of nano SiO2-PVA composite films *Opt. Mater. (Amst).* **90** 139–44
[43] Jiang M, Ding Y, Zhang H, Ren J, Li J, Wan C and Hong Y 2020 A novel ultrathin single-crystalline Bi 2 O 3 nanosheet wrapped by reduced graphene oxide with improved electron transfer for Li storage *J. Solid State Electrochem.* **24** 2487–97
[44] Abdel-salam A I, Gomaa I, Khalid A and Soliman T S 2022 Investigation of raman spectrum , structural , morphological , and optical features of Fe2O3 and Fe2O3/reduced graphene oxide hybrid nanocomposites *Phys. Scr.* **97** 125807
[45] Soliman T S, Vshivkov S A, Abdel-salam A I, Gomaa I and Khalid A 2023 Structural and optical parameters of polyvinyl alcohol fi lms reinforced with Mn 2 O 3 / reduced graphene oxide composite *Phys. Scr.* **98** 15832
[46] Huang K, Yu H, Xie M, Liu S and Wu F 2019 Effects of poly(ethylene glycol)-grafted graphene on the electrical properties of poly(lactic acid) nanocomposites *RSC Adv.* **9** 10599–605
[47] Yang C C, Lee Y J, Chiu S J, Lee K T, Chien W C, Lin C T and Huang C A 2008 Preparation of a PVA/HAP composite polymer membrane for a direct ethanol fuel cell (DEFC) *J. Appl. Electrochem.* **38** 1329–37
[48] Ho C, Chan C, Huang Y and Tien L 2013 The study of optical band edge property of bismuth oxide nanowires α -Bi2O3 *Opt. Express* **21** 9658–9
[49] Saguì N A, Ström P, Edvinsson T and Pehlivan I B 2022 Nickel site modification by high-valence doping: effect of tantalum impurities on the alkaline water electro-oxidation by NiO probed by operando raman spectroscopy *ACS Catal.* **12** 6506–16
[50] Mironova-Ulmane N, Kuzmin A, Sildos I, And L P and Grabis J 2019 Magnon and phonon excitations in nanosized NiO *Latv. J. Phys. Tech. Sci.* **56** 61–72
[51] Morimune S, Nishino T and Goto T 2012 Poly (vinyl alcohol)/ graphene oxide nanocomposites prepared by a simple eco-process *Polym. J.* **44** 1056–63
[52] Aslam M, Kalyar M A L I and Raza Z A L I 2018 Investigation of zinc oxide-loaded poly (vinyl alcohol) nanocomposite films in tailoring their structural , optical and mechanical properties *J. Electron. Mater.* **47** 3912–26
[53] Abdelaziz M and Ghannam M M 2010 Influence of titanium chloride addition on the optical and dielectric properties of PVA films *Phys. B Phys. Condens. Matter.* **405** 958–64
[54] Abul-Magd A A, Morshidy H Y and Abdel-Ghany A M 2020 The role of NiO on the structural and optical properties of sodium zinc borate glasses *Opt. Mater. (Amst).* **109** 110301

[55] Soliman T S, Rashad A M, Ali I A, Khater S I and Elkalashy S I 2020 Investigation of linear optical parameters and dielectric properties of polyvinyl alcohol/ZnO nanocomposite films *Phys. Status Solidi Appl. Mater. Sci.* **217** 2000321
[56] Khairy Y, Yahia I S and Elhosiny Ali H 2020 Facile synthesis, structure analysis and optical performance of manganese oxide-doped PVA nanocomposite for optoelectronic and optical cut-off laser devices *J. Mater. Sci., Mater. Electron.* **31** 8072–85
[57] Salem A M, Mohamed A R, Abdelghany A M and Yassin A Y 2022 Effect of polypyrrole on structural, optical and thermal properties of CMC-based blends for optoelectronic applications *Opt. Mater. (Amst).* **134** 113128
[58] Zaki M F, Tayel A and El Basaty A B 2022 Tuning the optical properties, AC conductivity and dielectric modulus of PVA membrane by inclusion of TiO2 nanoparticles *Bull. Mater. Sci.* **45** 236
[59] Yassin A Y 2023 Synthesized polymeric nanocomposites with enhanced optical and electrical properties based on gold nanoparticles for optoelectronic applications *J. Mater. Sci., Mater. Electron.* **34** 46
[60] Alhassan S, Alshammari M, Alshammari K, Alotaibi T, Alshammari A H, Fawaz Y, Abdel T, Taha M and Henini M 2023 Preparation and optical properties of PVDF-CaFe2O4 polymer nanocomposite films *Polymers (Basel).* **15** 2232
[61] Aziz S B, Ahmed H M, Hussein A M, Fathulla A B, Wsw R M and Hussein R T 2015 Tuning the absorption of ultraviolet spectra and optical parameters of aluminum doped PVA based solid polymer composites *J. Mater. Sci., Mater. Electron.* **26** 8022–8
[62] Krishnakumar V, Ranjith R, Jayaprakash J, Boobas S and Venkatesan J 2017 Enhancement of photocatalytic degradation of methylene blue under visible light using transparent Mg-doped CdS–PVA nanocomposite films *J. Mater. Sci., Mater. Electron.* **28** 13990–9
[63] Alharthi S S, Alzahrani A, Razvi M A N, Badawi A and Althobaiti M G 2020 Spectroscopic and Electrical Properties of Ag2S/PVA Nanocomposite Films for Visible-Light Optoelectronic Devices *J. Inorg. Organomet. Polym. Mater.* **30** 3878–85